High Throughput Ultrasonic Multi-implant Readout Using a Machine-Learning Assisted CDMA Receiver

Sina Faraji Alamouti*, Mohammad Meraj Ghanbari*, Nathan Tessema Ersumo, and Rikky Muller

***Abstract*— Untethered, wireless peripheral nerve recording for prosthetic control requires multi-implant communications at high data rates. This work presents a multiple-access ultrasonic uplink data communication channel comprised of 4 free-floating implants and a single-element external transducer. Using code-division multiple access (CDMA), overall channel data rates of up to 784 kbps were measured, and a machine-learning assisted decoder improved BER by >100x. Compared with prior art, this work incorporates the largest number of implants at the highest data rate and spectral efficiency reported.**

***Index Terms*— CDMA, implant, machine learning, neural network, peripheral nerve interface, ultrasound, wireless data.**

I. Introduction

Recording neural activity from the residual nerves is a gateway to restoring post-amputation loss of motor function. Short-term human studies have previously demonstrated active control of prosthetic arms using recorded neural signals from the peripheral nervous system (PNS) [1], [2], [3], [4]. It has been shown that increasing the number of recording sites on *different* neural pathways, (e.g. medial and ulnar nerves), provides considerably more controllable degrees of freedom on the prosthetic arm, translating into more natural hand gestures. Due to the use of tethered electrodes in previous studies, (e.g. Utah Slanted Electrode Arrays), the quality of the recorded signals degraded over time; in part due to widening of the dead-zones in the vicinity of the electrodes [5]. On the other hand, free-floating electrodes have shown excellent signal quality over time [6]. Therefore, a distributed network of free-floating peripheral nerve recording implants is proposed and illustrated in Fig. 1.

The development of the interface shown in Fig. 1 presents a number of challenges. To minimize infection risk, tissue damage and improve the ease of implantation, the implants should be wireless and as small as possible. The bandwidth of spiking nerve signals necessitates an uplink data rate of ∼200 kbps (∼10 bits/S at 20 kS/s) for each implant. And lastly, for deep targets on the PNS, wireless operation range, including power delivery to implants, of 10s of mm is required.

Compared with batteries and electromagnetic power transfer, ultrasound (US) has been demonstrated to provide the highest power delivery density to miniaturized (mm- and sub-mm-scale) implants operating at depth (up to 120 mm [7]) in tissue [8]. Due to relatively low ultrasound carrier frequencies (1–5 MHz), and the limited power budget of implants (resulting in low SNR), achieving uplink data rates of ∼200 kbps/implant is challenging and has not been achieved in the art to our knowledge. To meet the requirements of a practical neural interface [4], tens of neural recording sites are needed, resulting in a required total data rate of 2–20 Mbps.

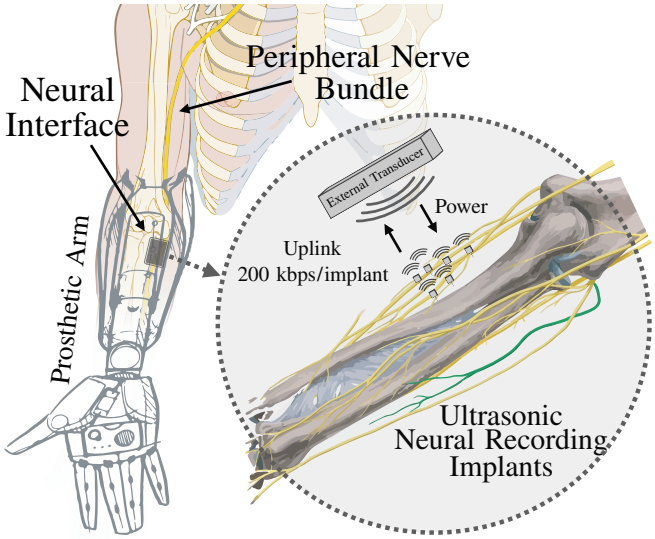

Fig. 1: Concept of active prosthetic arm control using a distributed network of ultrasonically powered peripheral nerve implants.

This work focuses on the demonstration of high-throughput data uplink rather than low-noise acquisition of neural signals. We present an ultrasonic uplink protocol and receiver that achieves a total data rate of 784 kbps for 4 implants (196 kbps/implant) and a spectral efficiency of 490 kbps/MHz, the highest reported to our knowledge. Further scaling of this protocol to support up to 12 implants at 2.45 Mbps is possible, as discussed in Section IV.

Section II discusses design challenges and strategies to realize an ultrasound multi-access high data-rate uplink communication channel. Experimental results are presented in Section III. Finally, comparison with the state-of-the-art is summarized in Section IV.

II. US Power and Uplink Data Protocols

Bulk piezoceramic (piezo) resonators are ultrasound transducers that are commonly used as both implant energy harvesters and data transmitters/receivers [9], [10]. Since bulk piezos dominate the volume of the implants, it is desirable to reduce the number of piezos to one per implant. In a *single-piezo* implant, there exist two previously reported schemes that perform both power delivery and uplink data transmission: (a) sequential power harvesting followed by

*Equally-Credited Authors
All authors are with the Department of Electrical Engineering and Computer Sciences, University of California, Berkeley, Berkeley, CA 94720, USA . ({sina_faraji, ghanbari}@berkeley.edu)

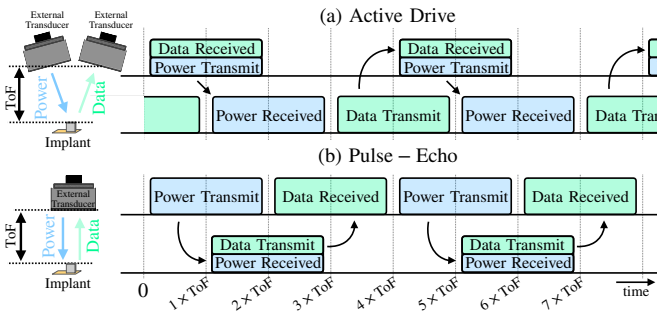

Fig. 2: Previously reported power and uplink protocol for single-piezo implant devices. (a) active drive: sequential power harvesting and uplink data transmission (b) pulse-echo scheme: simultaneous power harvesting and uplink echo modulation.

active drive [7] and (b) simultaneous power harvesting and echo modulation [12]. In both of the schemes, the US power pulse is generated by a distant external transducer. Case (a) requires an additional transducer for receiving data as illustrated in Fig. 2(a). In case (a), once the power harvesting phase is over and energy is stored on a capacitor, the implant piezo is actively driven by the implant circuit to transmit data back to the second external transducer where it is acquired and subsequently demodulated and post-processed. In case (b), known as the pulse-echo scheme, uplink data transmission is realized by modulating the amplitude of the echo of the power delivery pulse, Fig. 2(b). In the pulse-echo scheme, the modulated echo carrying uplink data is received by the same external transducer that initially transmitted the power pulse. Therefore, to avoid an excessive dynamic range requirement of the analog front-end of the receive chain, the pulse/echo duration is restricted to twice that of the time of flight (ToF) between the external transducer and the implant resulting in a 50% duty cycle for data transmission. Although the data transmission period of the active drive scheme is not constrained by the ToF, actively driving the piezo rapidly discharges the implant charge-reservoir and consequently must be short, usually <50% of the time, and immediately followed by another power pulse. Therefore, in this work, a generic protocol-independent, 50%-duty-cycled data transmission period is considered.

A. Multiple-Access Protocols

The two schemes described above can be extended to achieve multi-implant communications. Multi-site ultrasound power delivery has been previously demonstrated by ultrasound phased-arrays [11] or a single-element external transducer [12], an apparent tradeoff between high spatial selectivity and low cost. In either case, power is delivered to the implants during pre-determined time slots shared between all implants. A significantly more challenging problem in a multi-implant setting is the simultaneous uplink data transmission. Classic RF multiple access communication protocols, namely frequency-division multiple access (FDMA), time-division multiple access (TDMA), and code-division multiple access (CDMA) are possible options.

Implementation of US FDMA has a practical limitation that every implant piezo in the network needs to have a precise and unique geometry (e.g. thickness), increasing

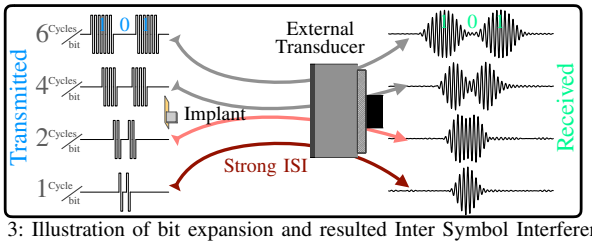

Fig. 3: Illustration of bit expansion and resulted Inter Symbol Interference (ISI): transmission of a '101' for various cycles/bit configurations.

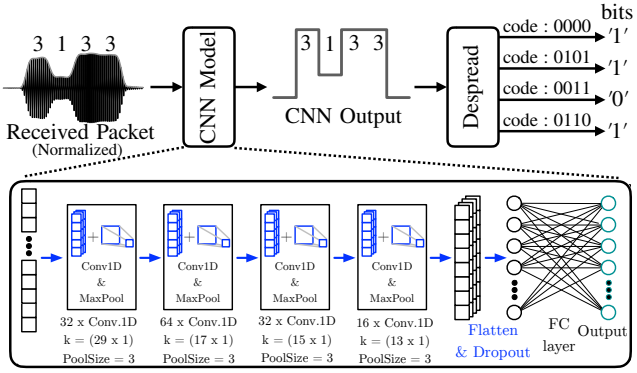

Fig. 4: Block diagram of machine-learning assisted CDMA decoder.

the implementation cost and complexity. Excellent uplink data transmission rates have been reported using TDMA for a network of two implants [11], but a potential scaling limitation of the TDMA is its sensitivity to multipath reflections, especially at high-data rates and/or high number of implants when the allotted time slot to each implant becomes too narrow such that a strong multipath reflection can contaminate other channels. In an US CDMA network, all implant piezos share the same geometrical design [12], and the channel sensitivity to multipath reflections can be significantly reduced by using a simple multipath-correlator receiver, e.g. Rake [13]. Also, similar to cellular CDMA, the intermittent neural signal can be exploited (by squelching) to enhance the bit error rate (BER) at high data rates [14]. Thus, CDMA is an attractive protocol for multi-site implant communications and is therefore considered in this work.

B. Machine Learning Assisted CDMA Decoder

The data transmission period (each packet length) is of finite duration limited by the ToF. Since the packet transmission rate is also set by the ToF, increasing the data rate requires increasing the number of bits transmitted in each packet, resulting in fewer US cycles/bit. For instance for a packet length of 60 μs, 96 cycles of a 1.6 MHz carrier are available. Transmitting 16 and 96 bits/packet respectively results in allocation of 6 and 1 US cycles/bit. Fewer cycles per transmitted bit consequently result in inter-symbol interference (ISI). Fig. 3 shows signals received by the external transducer when an implant is transmitting a '101' for various numbers of cycles/bit, assuming that on-off keying (OOK) base-band digital modulation is used. Due to the finite mechanical bandwidth of the piezo, the received signal is expanded in time. It can be observed that as the number of cycles/bit decreases the transmitted bits are merged together and become indistinguishable from one another. This results in a strong ISI, which significantly degrades the BER at high data rates if a conventional decoder

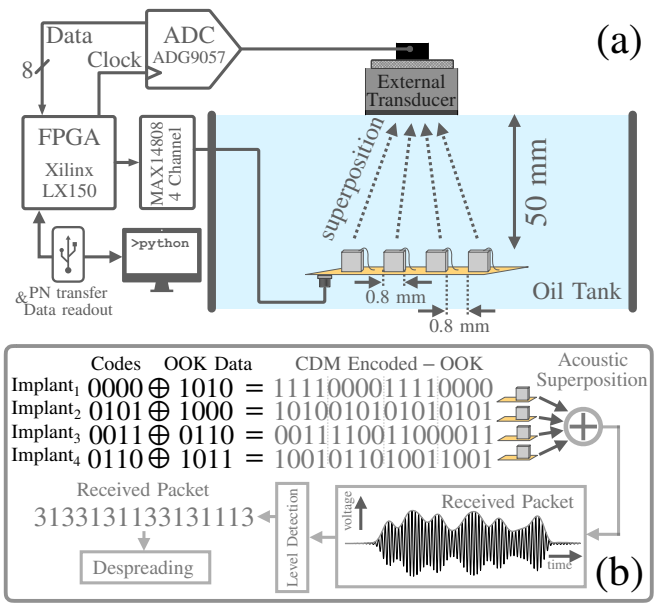

Fig. 5: (a) Setup for automated data collection and (b) generation .

is used. Here, we present an ISI tolerant machine learning (ML) assisted decoder to improve BER at high data rates.

Prior art has demonstrated the application of ML, especially Neural Networks (NN) in communication. [15] demonstrates that for a CDMA protocol, a NN approach can outperform conventional matched-filter implementations and deliver results close to that of an optimal decoder. In [16], an end-to-end approach was taken to enhance the performance of detectors for OOK and pulse amplitude modulation. Furthermore, bi-directional recurrent NN (RNN) model was shown to excel at continuous multi-symbol sequence detection in the presence of strong ISI.

In this work, the waveform of the packetized data is used to train the ML model. Each packet forms an image that includes all transition levels through the symbols in that packet. 1-D image processing is performed by a Convolutional Neural Network (CNN) that processes the raw waveform, eliminating the need for manually selecting input features. A CNN-based model benefits from parameter sharing to detect certain features that can appear anywhere along the image; as a result, fewer model parameters are required to achieve the desired patter recognition accuracy, relaxing the data size and training time constraints.

Fig. 4 shows a block diagram of the receiver backend. The raw acquired waveform is input to a CNN-based regressor, with no prior filtering or demodulation. The CNN model is comprised of 4, 1-D Conv. layers with ReLU activation function, followed by Max Pooling operations and a final fully connected (FC) layer that maps to the outputs. The CNN is trained to predict the corresponding stream of CDMA levels. These arrays of predicted levels are then despread (using the assigned CDMA codes) to recover the actual data transmitted by each implant.

III. Experimental Results

To experimentally verify the efficacy of the ML-assisted decoder and specify the maximum achievable data rate, the

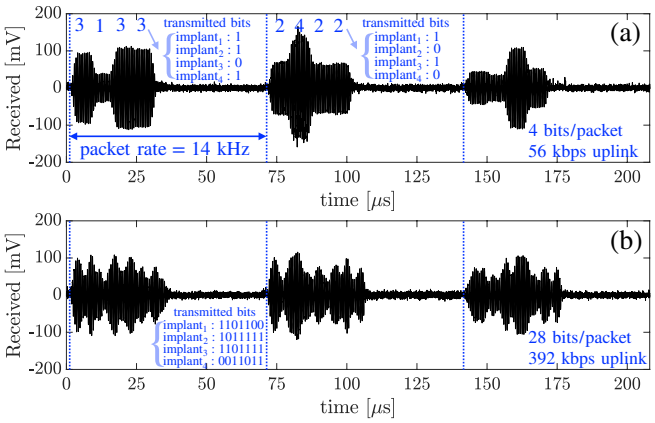

Fig. 6: Simultaneous data transmission of 4 implants using OOK CDMA modulation. Measured waveforms received by external transducer for data rates of (a) 56 kbps and (b) 392 kbps.

setup shown in Fig. 5 was used for automated data generation and collection. Pseudorandom OOK data generation and CDM encoding was performed on a PC. Four piezoceramic cubes (APC851, 0.51 mm^3, 1.6 MHz) mounted on a flexible board (0.3 mm thick) were suspended at a distance of 50 mm away from a 0.5″ diameter single-element unfocused external transducer (Olympus V304-SU-F1.88IN-PTF) in oil (with ∼0.5 dB/cm at 2 MHz). Each piezo was driven by an ultrasound pulser (Maxim, MAX14808) whose command inputs were controlled by an FPGA (Xilinx Spartan-6 LX150) clocked at 57 MHz. CDM-encoded OOK pseudorandom data was generated by a PC and transferred to the FPGA for each packet of data. Once the packets are launched by driving the implant piezos, the output of the external transducer is sampled by an 8-bit analog to digital converter (ADG9057) to record the acoustically superimposed CDM-encoded data transmitted by all piezos. The recorded signal at the output of the external transducer was transferred to PC where labeling and subsequent digital processing were performed. Measurements were made for multiple data rate configurations at 10,000 packets per configuration. A set of 4,000 packets (∼290 ms of recording) were used for model training. For the two highest data rate configurations, 6400 packets were used instead for training the CNN as in these configurations packets contained a significantly higher number of bits to be decoded. Pre-trained models and transfer learning techniques can be used to further shorten the training phase. All the measurements were performed with a 50% packet rate as explained in Section II. Since ToF is held constant, packet data transmission rate was set to 14 kHz, and the packet duration was maintained at 35 μs (56 ultrasound cycles at 1.6 MHz). The data rate was adjusted by changing the number of bits/implant per packet from 1 to 14, respectively resulting in 56 kbps to 784 kbps data rates. Measured packet streams received by the external transducer for 56 kbps and 392 kbps uplinks are shown in Fig. 6(a) and (b). The transition levels (superimposed codes transmitted by implants, e.g. 3133) for low data rates, e.g. 56 kbps in Fig. 6(a), are clearly visible. In Fig. 6(b), however, transition levels due to strong ISI cannot be easily observed.

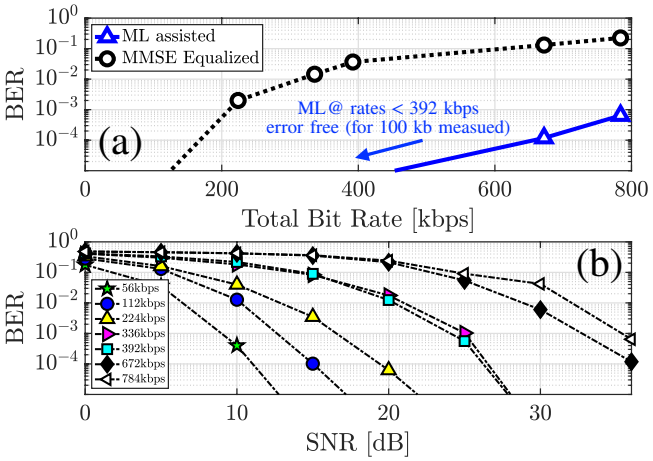

Fig. 7: (a) Measured bit error rate (BER) vs. total data rate of the channel. (b) Measured bit error rate (BER) vs. received signal-to-noise (SNR) ratios for various total channel data rates.

TABLE I: Comparison of Recently Published US Links

	[9]	[17]	[7]	[18]	[11]	**This work**	**This work**	**This work**
No. of Implants	2	1	1	1	2	**4**	**4**	**4**
Piezos per Implant	1	2	1	2	2	**1**	**1**	**1**
External Elements	32	2	2	2	32	**1**	**1**	**1**
Depth [mm]	60	85	120	37.5	65	**50**	**50**	**50**
f_c [MHz]	1	2.5	0.79	1	2.52	**1.6**	**1.6**	**1.6**
Uplink [kbps]	50	100	10	75	194	**392**	**672**	**784**
SE* [kbps/MHz]	50	40	12.6	75	77	**245**	**420**	**490**
BER	–	1E-4	1E-5	–	1E-4	**1E-5**	**1.2E-4**	**6.4E-4**

*Spectral Efficiency

The measured BER for different channel data rate configurations is shown in Fig. 7(a) for a signal-to-noise ratio (SNR) of 35 dB. A comparison was made with a more conventional approach, a Minimum Mean-Squared Error (MMSE) detector, which was implemented, trained and tested on the same data set. At low data rates where ISI is insignificant, both of the decoders can achieve a BER of 1E-5. As the data rate increases, ISI significantly degrades the performance of the MMSE decoder. An optimal CDM decoder [13] could enhance this performance, but such an implementation would be computationally impractical for data rates greater than 224 kbps. The ML-assisted decoder achieves a BER better than 6.4E-4 for data rates up to 784 kbps without the computational complexity of an optimal CDM decoder. To evaluate the system performance in lower SNR values, in-band gaussian noise was added to the collected samples to generate an SNR range of 0-35 dB. At each SNR level, the model was retrained with noisy samples and retested with the data set. Fig. 7(b) summarizes the achieved BER by the ML-assisted CDMA decoder at different rates and SNR values. As an example, for 30 dB of SNR, BER of 5E-7 can be achieved for data rates up to 392 kbps.

IV. Summary

Table I summarizes the performance metrics of the CDMA communication channel presented in this work compared to those of the prior art. This work incorporates 4 single-piezo implants operating at a total data rate of 784 kbps, the highest reported to our knowledge. Introducing a CNN-assisted CDMA receiver improves BER by more than 2 orders of magnitude when compared with a common MMSE decoder. This work also achieves the highest reported spectral efficiency $\sim$10$\times$ higher than the best reported single-piezo implant [9], and $\sim$6.4$\times$ higher than the best dual-piezo implant[11]. Moderate carrier scaling to 5 MHz would increase the number of implants supported in this work to 12, resulting in an overall channel datarate of 2.45 Mbps.

Acknowledgment

The authors thank the Hellman Fellows Fund and the sponsors of the Berkeley Wireless Research Center. The authors also thank Prof. Anant Sahai, Prof. Michel Maharbiz, Prof. Jose Carmena, and Alan Dong for technical discussion.

References

[1] G. S. Dhillon *et al.*, "Residual function in peripheral nerve stumps of amputees: implications for neural control of artificial limbs," *The Journal of hand surgery*, vol. 29, no. 4, pp. 605–615, 2004.

[2] P. M. Rossini *et al.*, "Double nerve intraneural interface implant on a human amputee for robotic hand control," *Clinical neurophysiology*, vol. 121, no. 5, pp. 777–783, 2010.

[3] T. Davis *et al.*, "Restoring motor control and sensory feedback in people with upper extremity amputations using arrays of 96 microelectrodes implanted in the median and ulnar nerves," *Journal of neural engineering*, vol. 13, no. 3, p. 036001, 2016.

[4] S. Wendelken *et al.*, "Restoration of motor control and proprioceptive and cutaneous sensation in humans with prior upper-limb amputation via multiple utah slanted electrode arrays (useas) implanted in residual peripheral arm nerves," *Journal of neuroengineering and rehabilitation*, vol. 14, no. 1, p. 121, 2017.

[5] F. Pothof *et al.*, "Comparison of the in-vivo neural recording quality of floating and skull-fixed silicon probes," in *2017 8th International IEEE/EMBS Conference on Neural Engineering*, 2017, pp. 158–161.

[6] A. Ersen *et al.*, "Chronic tissue response to untethered microelectrode implants in the rat brain and spinal cord," *Journal of neural engineering*, vol. 12, no. 1, p. 016019, 2015.

[7] M. Weber *et al.*, "A miniaturized single-transducer implantable pressure sensor with time-multiplexed ultrasonic data and power links," *Journal of Solid-State Circuits*, vol. 53, no. 4, pp. 1089–1101, 2018.

[8] D. K. Piech *et al.*, "A wireless millimetre-scale implantable neural stimulator with ultrasonically powered bidirectional communication," *Nature Biomedical Engineering*, vol. 4, no. 2, pp. 207–222, 2020.

[9] M. L. Wang *et al.*, "Closed-loop ultrasonic power and communication with multiple miniaturized active implantable medical devices," in *2017 IEEE International Ultrasonics Symposium*, 2017, pp. 1–4.

[10] M. M. Ghanbari *et al.*, "17.5 a 0.8 mm 3 ultrasonic implantable wireless neural recording system with linear am backscattering," in *2019 IEEE International Solid-State Circuits Conference-(ISSCC)*. IEEE, 2019, pp. 284–286.

[11] T. C. Chang *et al.*, "Multi-access networking with wireless ultrasound-powered implants," in *2019 IEEE Biomedical Circuits and Systems Conference (BioCAS)*. IEEE, 2019, pp. 1–4.

[12] M. M. Ghanbari *et al.*, "A sub-mm 3 ultrasonic free-floating implant for multi-mote neural recording," *IEEE Journal of Solid-State Circuits*, vol. 54, no. 11, pp. 3017–3030, 2019.

[13] D. Torrieri, *Principles of spread-spectrum communication systems*. Springer, 2005, vol. 1.

[14] K. Gilhousen *et al.*, "On the capacity of a cellular cdma system," *IEEE Transactions on vehicular technology*, vol. 40, no. 2, 1991.

[15] B. Aazhang *et al.*, "Neural networks for multiuser detection in code-division multiple-access communications," *IEEE Transactions on Communications*, vol. 40, no. 7, pp. 1212–1222, 1992.

[16] N. Farsad *et al.*, "Neural network detection of data sequences in communication systems," *IEEE Transactions on Signal Processing*, vol. 66, no. 21, pp. 5663–5678, 2018.

[17] T. C. Chang *et al.*, "27.7 a 30.5 mm 3 fully packaged implantable device with duplex ultrasonic data and power links achieving 95kb/s with <10-e4 ber at 8.5 cm depth," in *2017 IEEE International Solid-State Circuits Conference (ISSCC)*. IEEE, 2017, pp. 460–461.

[18] M. Meng *et al.*, "Gastric seed: Toward distributed ultrasonically interrogated millimeter-sized implants for large-scale gastric electrical-wave recording," *IEEE Transactions on Circuits and Systems II: Express Briefs*, vol. 66, no. 5, pp. 783–787, 2019.